Hindawi
Journal of Nanotechnology
Volume 2023, Article ID 1292762, 12 pages
https://doi.org/10.1155/2023/1292762

Research Article

Photo-Oxidation of Organic Dye by Fe_2O_3 Nanoparticles: Catalyst, Electron Acceptor, and Polyurethane Membrane ($PU\text{-}Fe_2O_3$) Effects

Bachir Yaou Balarabe,[1] **Maman Nasser Illiassou Oumarou**,[2] **Abdoul Salam Koroney**,[3] **Irédon Adjama**,[2] **and Abdoul Razak Ibrahim Baraze**[4]

[1]*Mining Engineering and Environment Department, Higher Institute of Mining,Industry and Geology, Emig-Bp, Niamey 11583, Niger*
[2]*School of Pharmacy, National Forensic Sciences University, Sector-09, Gandhinagar 382007, India*
[3]*Département Science de l'Environnement, Faculté des Science Agronomiques, Université Boubakar Bâ de Tillabéri, BP 175, Tillabéri, Niger*
[4]*Champollion National University Institute, Albi Campus University Library of Albi, Albi, France*

Correspondence should be addressed to Bachir Yaou Balarabe; yaoubalarabe@gmail.com

Received 15 November 2022; Revised 20 January 2023; Accepted 27 January 2023; Published 17 February 2023

Academic Editor: Jagpreet Singh

The textile industry's discharges have long been regarded as severe water pollution. The photocatalytic degradation of dyes using semiconductors is one of the crucial methods. The present study efficiently used the mechanical method to synthesize Iron oxide Nanoparticles. XRD, FT-IR, UV-Vis DRS, and Raman analyses were performed to analyze the structural and optical. From the data provided by XRD and Raman data, we believed that the as-synthesized Iron oxide was pure hematite (α-Fe_2O_3) with a hexagonal structure. Additionally, the EDS results show that the synthesized material is pure. By adjusting specific parameters, including the dye concentration, the catalyst dosage, the pH, and the oxidizing agent such as H_2O_2 and $K_2S_2O_8$, the degradation of eosin yellowish using Fe_2O_3 as a photocatalyst has been discussed. Additionally, the kinetics of eosin yellowish degradation has been studied. A study was also conducted using Fe_2O_3 nanoparticles attached to polyurethane polymer (PU) to investigate its photocatalytic activity on methylene blue, methyl orange, and indigo carmine. In 30 minutes, nearly 90% of the dyes had degraded. The total organic carbon (TOC) analysis confirmed this result.

1. Introduction

The fast growth of the social economy and industrialization results in hundreds of new pollutants being released into the environment, causing massive damage [1]. Dye is used in many sectors, such as dyeing, printing, beauty care products, medications, calfskin, printing ink, and fluorescent color. Most Dyes are natural carcinogens, and their release into the environment as wastewater is a significant source of visual contamination, eutrophication, and disruption of aquatic life [2]. Eosin yellow, also known as 2-(2,4,5,6-Tetrabromo-6-oxido-3-oxido-3H xanthenes-9-yl) benzoate disodium salt, is an anionic dye. According to toxicological writings on eosin yellow, the dye can cause severe skin and eye irritation. When it comes into contact with the skin, it causes irritation, redness, and inconvenience. When consumed, it has various adverse effects, most notably on vital organs such as the liver and kidneys. The retinal ganglion cell, found on the retina's internal surface, can be permanently damaged when eosin yellowish comes into direct contact with the eye. Additionally, it destroys DNA in the digestive systems of living things, causing various human disorders [3–7]. Numerous improvements in wastewater treatment have been made over the decade, including electrochemical treatment, oxidation,

ozonation, and photochemical treatment. A standard method for degrading harmful substances has been photocatalytic degradation driven by semiconductors. In essence, photodegradation begins with the formation of electron/hole pairs in the semiconductor as a result of light absorption with energy comparable to or more potent than the bandgap [8]. TiO_2 and ZnO are two of the few semiconductors used in photocatalysis. They both have high photosensitivity, especially in the UV range, suggesting that they can effectively drive the oxidation and reduction processes. Despite their exceptional qualities, the semiconductors, as mentioned above, have significant disadvantages, such as fast charge transporter recombination and large bandgap [8, 9]. A new era of materials responding to a wide range of wavelengths has overcome these limitations. The solution can ideally be the solution for the photocatalytic activity of a material with a suitable crystal structure, surface area, size distribution, porosity, ideal bandgap, and magnetic property. Iron oxides, including Fe_3O_4 (magnetite), α-Fe_2O_3, β-Fe_2O_3, Υ-Fe_2O_3, FeO, and spinel ferrites (MFe_2O_4), relatively cheap and stable, have earned much interest in the field of photocatalysis are one of them [10, 11]. Additionally, it is well known that magnetic iron oxides can be used as an efficient visible-light semiconductor photocatalyst due to their low bandgap, high conductivity, and high catalytic activity in the visible light region [12, 13]. For example, α-Fe_2O_3 nanoparticles could altogether remove an aqueous solution of Rose Bengal within a short time [14]. Liu et al. used chemical solutions to prepare a porous Fe_2O_3, and the degradation efficiency was approx. 86.4% for the degradation of rhodamine B [15]. According to Deng et al., the electrospinning synthesized α-Fe_2O_3 nanowires could remove 85% of a highly concentrated solution of rhodamine B [16]. Several methods/techniques have recently been used to synthesize Iron Oxide nanoparticles, among them surfactant-assisted hydrothermal, microemulsion, and many other ways [8, 17–19]. Developing a reusable catalyst for treating dye-contaminatedstill-water bodies under visible light would also be very attractive [20–22]. By immobilizing nanomaterials on porous solid substrates, it is possible to improve their recyclability and efficiency [22]. According to Zhang et al., PVDF/GO/ZnO composite membranes have been shown to degrade methylene blue in water [23]. There are several membrane substrates available; however, polyurethane (PU) is one of the most promising materials because it is simple to process, versatile, and easily functionalized [24]. Per our survey, mechanical techniques such as grinding are among the most advantageous methods because of their simple procedure and low chemical consumption. In this study, α-Fe_2O_3 nanoparticles reported elsewhere were used to remove eosin yellow under visible light irradiation. Additionally, Fe_2O_3 nanoparticles attached to polyurethane polymer (PU) were investigated for their photocatalytic activity on methylene blue, methyl orange, and indigo carmine.

2. Experimental

2.1. Materials. All materials and solvents were obtained from commercial sources (Sisco Research Laboratories Pvt. Ltd., India, Sigma Aldrich, and Abhishek Enterprise Pvt. Ltd.) and used unchanged. Nonahydrate iron nitrate (extra pure, 99%), ammonium bicarbonate (extra pure AR, 99%), hydrogen peroxide (30%), sodium persulphate (extra pure, 99%), polyurethane foam, eosin yellowish, methylene blue, methyl orange and indigo carmine (dye content, ~99%). All measurements were performed with milli-Q water and spectroscopic-grade solvents. The optical properties measurements were carried out using a JASCO V.670 spectrophotometer for PL spectra, JASCO FT/4700 spectrophotometer for FT-IR spectra, and JASCO UV/VIS/NIR Spectrometer for UV-vis DRS analysis. The SEM images and EDS spectra were captured by using a field emission gun, a Nano Nova Scanning Electron Microscope (FEG-SEM) 450 with EDAX (FESEM) with an accelerating voltage ranging from 20V to 30 kV. Renishaw InVia Raman Spectroscopy was used to record Raman spectra. The X-ray diffraction pattern was measured using an X-ray diffractometer (GNR APD 2000 PRO) with a Cu-K light source. For the analysis of total organic carbon in treated dye solutions, OI Analytical Aurora model 1030, TOC instrument, was used.

2.2. Synthesis of Fe_2O_3 Nanoparticles. Fe_2O_3 nanoparticles were synthesized by grinding 2 g of iron nitrate with 1 g of Ammonium Bicarbonate route [25]. The reddish residue was washed several times with ethanol, followed by distilled water. The nanoparticles were collected, dried in a hot air oven at 100°C, and then calcined for 2 hours at 300°C. PU-Fe_2O_3 was synthesized by mixing 40 ml of polyurethane foam and 200 mg of Fe_2O_3 nanoparticles in accordance with the procedure shown in Figure 1.

2.3. Characterization

2.3.1. UV-Vis DRS Analysis. Using a JASCO V-670 spectrophotometer, the absorbance spectra of the as-prepared Fe_2O_3 nanoparticles were measured using UV-Vis diffused reflectance spectroscopy. The absorbance spectra from DRS measurements are shown in Figure 2(a), with maximum absorbance at 503 nm. The absorption edge of the nanoparticles synthesized demonstrates that the composites can be excited in the visible region. The spectra of the catalyst revealed a high absorbance with a direct bandgap of 1.5 eV (Figure 2(b)).

Fourier-transform infrared (FT-IR) spectroscopy was used to examine the detailed chemical interaction and quality of the as-prepared Fe_2O_3 nanoparticles. Figure 2(c) illustrates several well-defined absorption bands in the FTIR spectra. The absorption band at 3220.5 cm^{-1} is caused by the O-H stretching vibration of the H_2O molecule. The absorption band at 2275.5 cm^{-1} can be attributed to the triple bond between carbon and nitrogen (C≡N). The peaks at 1650.7 cm^{-1} and 995.0 cm^{-1} could be attributed to the organic solvent's alkenes (>C=C<) and C–O–C– vibrations. The signal at 809.9 cm^{-1} is most likely assigned to Fe–O stretching mode.

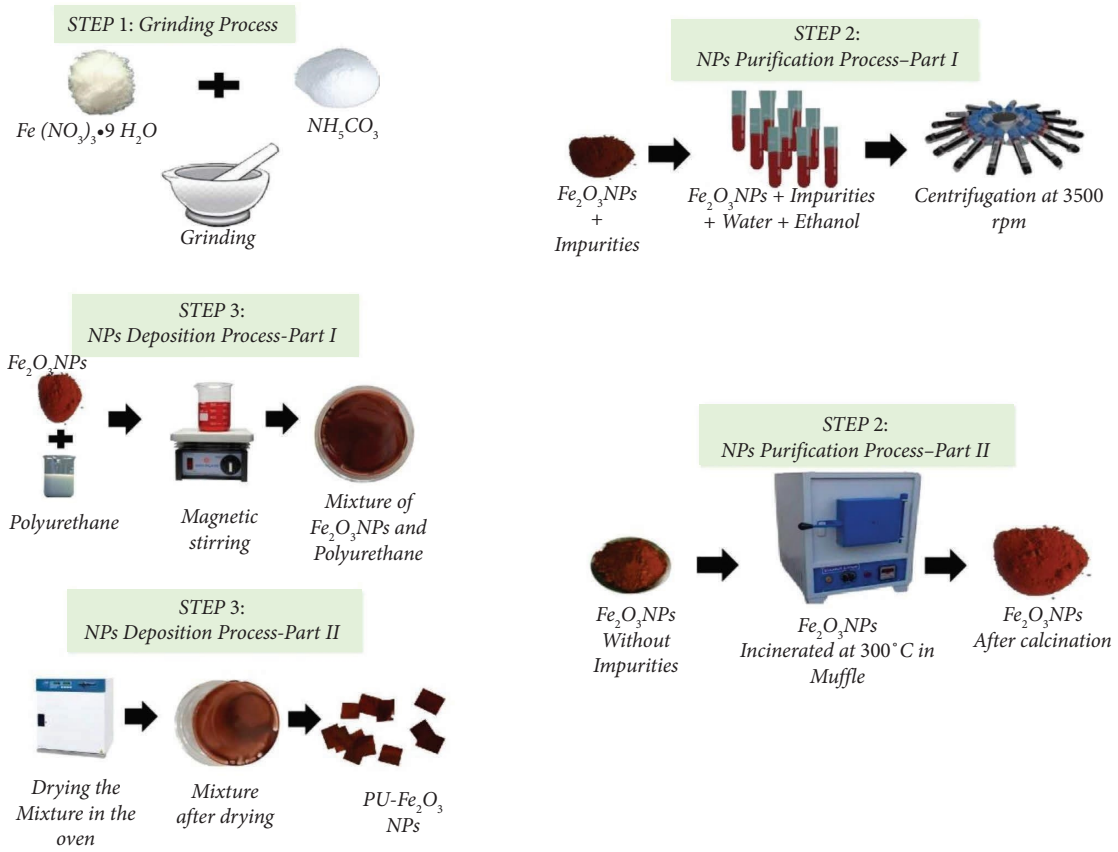

Figure 1: Synthesis of Fe_2O_3 nanoparticles and PU-Fe_2O_3 membrane.

To confirm the separation of photogenerated electrons and holes of the catalysts, the photoluminescence emission spectra of pure α-Fe_2O_3 were measured. The intensity of PL emission is well understood to be proportional to the rate of recombination of excited electron-hole pairs. Lower intensity indicates that more excited electrons are transferred or trapped, while higher intensity suggests that recombination occurs faster [26, 27]. At 250 nm excitation wavelength, α-Fe_2O_3 nanoparticles exhibit a narrow emission peak with a maximum of 688 nm (see Figure 2(d)). Rufus et al. achieved the same result when synthesizing α-Fe_2O_3 nanoparticles for antibacterial and nanofluid applications [28].

The X-ray diffraction (XRD) technique was used to assess the crystal structure, phase, and purity of as-synthesized material. Figure 3(a) illustrates all of the diffraction peaks in the XRD pattern of as-synthesized material peaks corresponding to (012), (104), (110), (113), (124), (116), (214), (300), and (208) lines in the XRD pattern are well matched with JCPDS file no 33-0664, indicating that the crystal system is pure hematite (α-Fe_2O_3). Furthermore, the diffraction pattern clearly shows that the XRD peaks are intense and broad, meaning that good crystalline and small-sizeα-Fe_2O_3 materials are formed. Scherer's formula (equation (1)) was used to calculate the size of crystallites in synthesized materials.

$$d = \frac{0.9\lambda}{\beta \cos\theta_B}, \tag{1}$$

where λ is the X-ray wavelength (1.54056), θ is the Bragg diffraction angle, and β is the line width at half the maximum of the most dominating peak. Using the above equation, the average crystallite size of the materials is 15.27 nm. The percent porosity of the iron nanoparticles was calculated using the following equation [29, 30]:

$$\text{percentage porosity} = 1 \times 100\%. \tag{2}$$

db and dx represent the X-ray density and bulk density, respectively. The percent porosity of iron oxide nanoparticles is 37.03%.

Raman spectroscopy measurements were used to analyze the chemical composition of the nanoparticle after synthesis. The Raman spectrum of a heavy metal oxide, such as Fe_2O_3, generally consists of four distinct features, which are as follows: Raman modes with low wavenumber (30–70 cm^{-1}), heavy metal ion vibrations (70–160 cm^{-1}), intermediate bridged anion modes (300–600 cm^{-1}), and nonbridging anion modes (>600 cm^{-1}) [31, 32]. The third and last categories are present in our sample. Figure 3(b) depicts the spectrum obtained from iron oxide nanoparticles in this study. Peaks at 221 cm^{-1}, 287 cm^{-1}, 405, 493 cm^{-1}, 608 cm^{-1}, and 1326 cm^{-1} correspond to α-Fe_2O_3. A peak at 659 cm^{-1} indicates the presence of a trace amount of Fe_3O_4. These Raman peaks are identical to those reported by a researcher [33]. According to the quantitative analysis by the EDS graph, the material has a relatively high

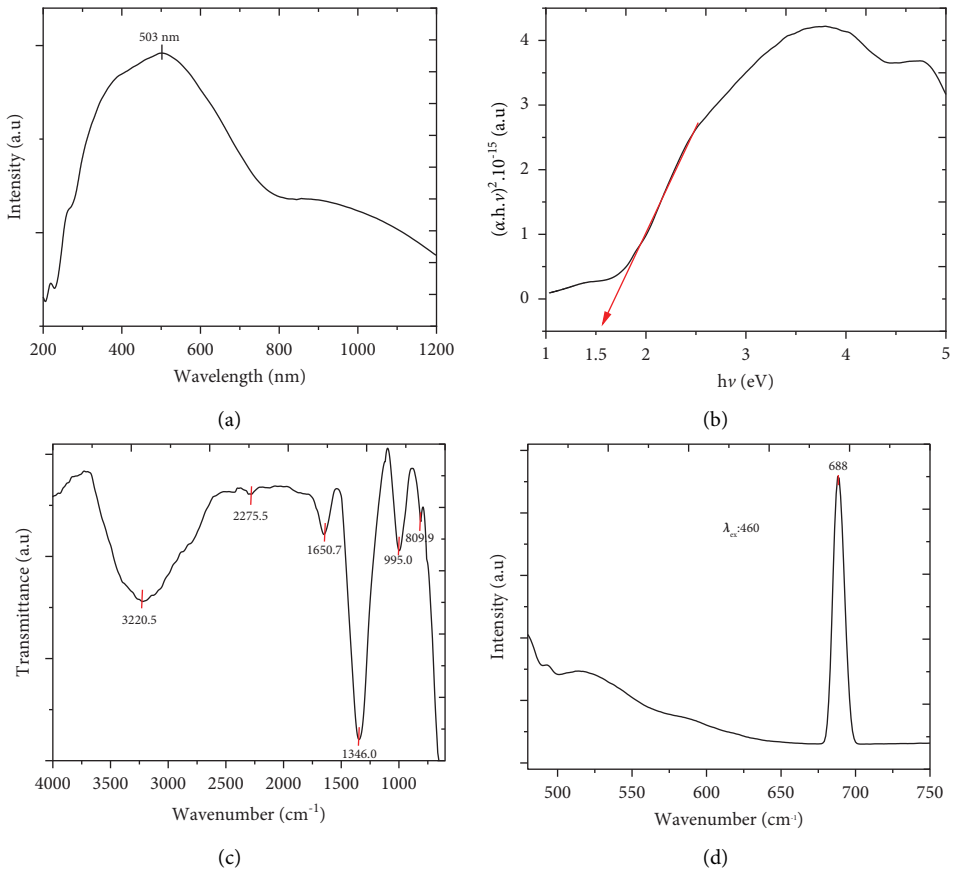

Figure 2: (a) UV-Vis diffuse reflectance spectra, (b) direct bandgap, (c) Fourier transform infrared analysis (FT-IR), and (d) photoluminescence spectra of Fe_2O_3 nanoparticles.

concentration of iron and oxygen. There were no other impurities found (Figure 3(c)).

The surface morphologies of the prepared samples were studied using a scanning electron microscope. Figure 4 shows an SEM image of a Fe_2O_3 nanoparticle. The image confirms the uniformity of the phase formation as well as the particle size. The nanoparticles are all spherical, ranging from 30 nm to 100 nm, with an average particle size of 66.84 nm.

2.4. Photocatalytic Activity Measurements. The photocatalytic performance of Fe_2O_3 nanoparticles in a photocatalytic reactor with visible lamp irradiation (High-pressure Mercury lamp, 125 watts) at room temperature was investigated. The photocatalytic reaction occurred in 500 ml closed flasks containing 200 ml of an aqueous solution of EY dye at a specific concentration of Fe_2O_3 nanoparticles. Before irradiation, the suspension was magnetically stirred in the dark for 15 minutes to achieve an adsorption-desorption equilibrium. At regular intervals, 1 mL aliquots from the flask were taken and mixed with 1 ml of deionized water, and the absorbance was measured with a spectrophotometer (Figure 5). The degradation efficiency of the photocatalyst can be expressed as follows:

$$\text{degradation efficiency}\,(\%) = \frac{(\text{C0} - \text{Ct})}{\text{C0}} * 100\%. \quad (3)$$

C_0 represents the dye concentration at adsorption equilibrium, and C_t represents the residual pollutant concentration at different illumination intervals [34–36]. Except for the effect of time exposure and the effect of the light source, which is 100 and 75 ppm for dye solution and catalyst quantity, respectively, the catalyst dose of 75 ppm and EY dye concentration of 75 ppm were chosen for the entire study.

2.4.1. Effect of the Light Source. To achieve a high degradation rate, the choice of a light source is an imperative parameter. For 100 ppm dye and 75 ppm iron nanoparticles, degradation occurs almost completely under visible light after 35 minutes of exposure; however, when exposed to visible light, it is reduced by half (Figure 6). This confirms the bandgap of the material obtained at 1.5 eV, which corresponds to the visible and near-infrared spectrums. According to Saquib and Muneer, independent of the parameters that contribute to degradation, the light source plays a crucial role in degradation [37].

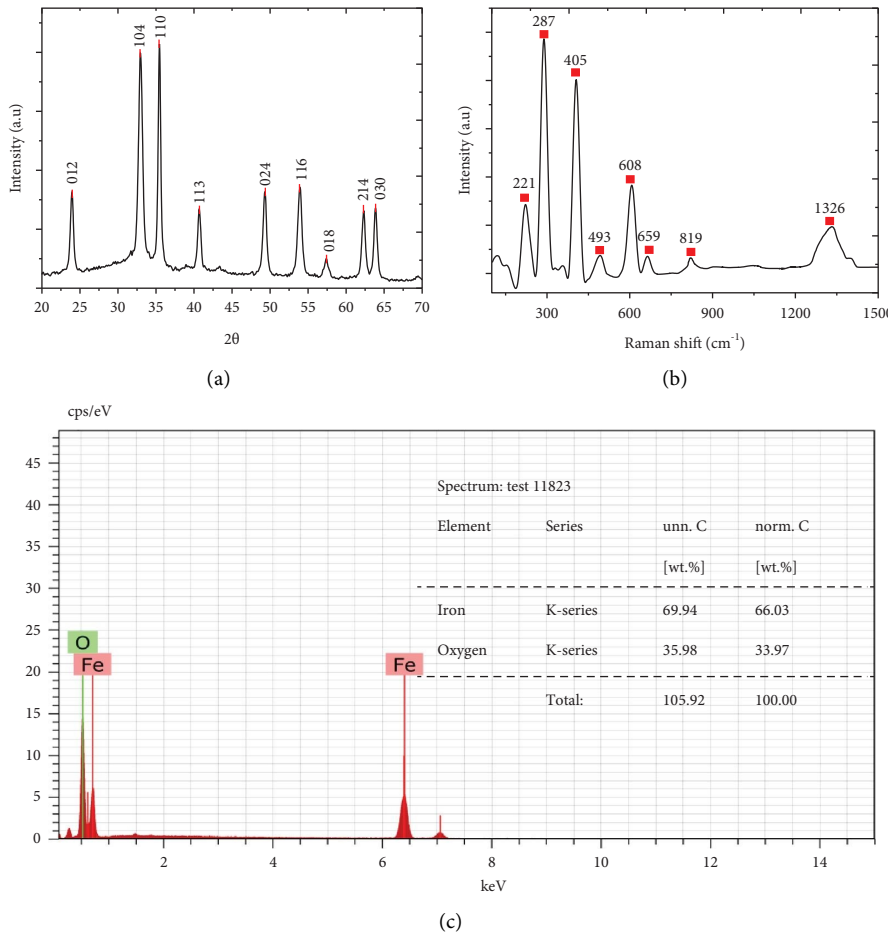

Figure 3: (a) XRD pattern, (b) Raman spectra, and (c) EDS pattern of synthesized α-Fe_2O_3 nanoparticles.

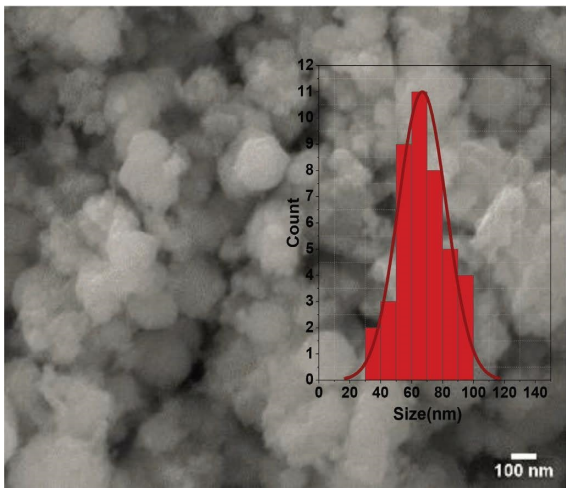

Figure 4: FESEM image (inset) nanoparticles size.

2.4.2. Effect of Dye Concentration. Trials with 25, 50, 75, and 100 ppm were performed to explore the influence of dye concentration. The dye concentration and catalyst were both set to 75 ppm. It was found that as the dye solution concentration increased, the photocatalytic degradation rate decreased gradually (Figure 7(a)). This could be due to more dye molecules being adsorbed on the outer layer of Fe_2O_3. As a result, this represses the activity of the particles, diminishing the receptive OH• and $O_2^{\bullet 2}$ free radicals attacking the dye molecules and photodegradation achievement. Increasing the initial dye concentration increases the chance of interactions between dye atoms and oxidizing species. Furthermore, due to the high dye concentration, a large amount of visible radiation may be consumed by dye molecules, reducing the amount of radiation penetrating the semiconductor. Finally, as the concentration of • OH and $O_2^{\bullet -}$ radicals decreases so does the effectiveness of the photocatalyst degradation response [38, 39].

2.4.3. Effect of Catalyst Dosage. In the presence of visible light, the effect of Fe_2O_3 dosage on color removal was investigated, as shown in Figure 7(b). Similarly, increasing the particle amount speeded up photodegradation. The maximum removal rate was obtained at 100 ppm Fe_2O_3. Following that, the rate declined to 150 ppm. This demonstrates that the catalyst dosage is an important variable affecting the photocatalytic dye's removal. The reduction occurred by increased suspension opacity caused by an abundance of Fe_2O_3 particles. The main reason is that light penetration is reduced by increasing the amount of photocatalyst.

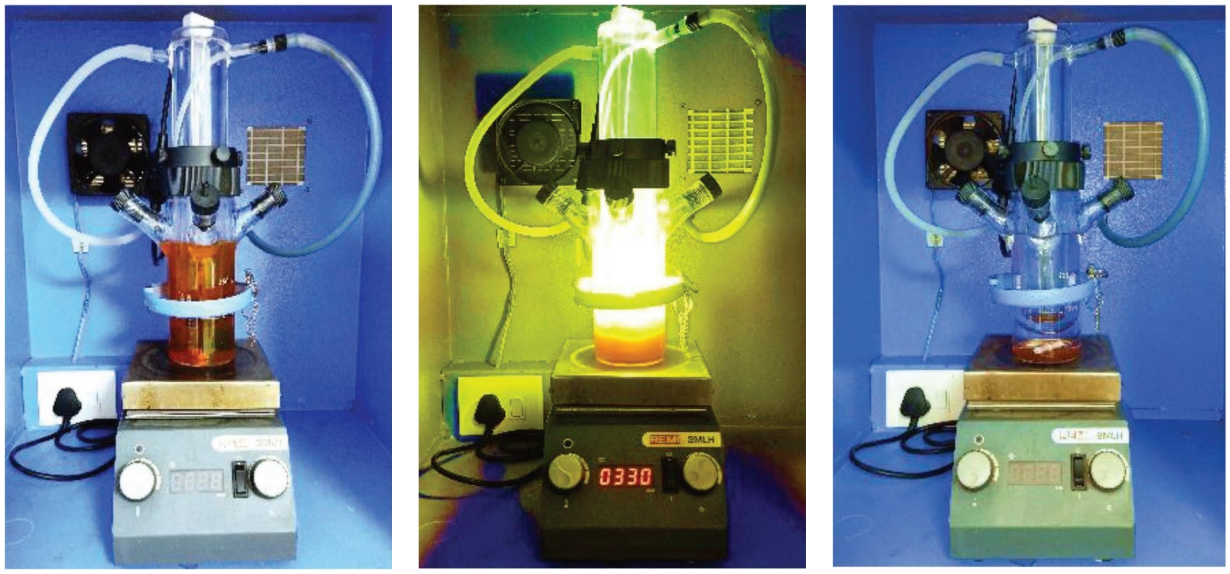

(a) (b) (c)

Figure 5: Photocatalytic reactor setup, (a) before treatment, (b) during treatment, and (c) after treatment of eosin yellowish dye.

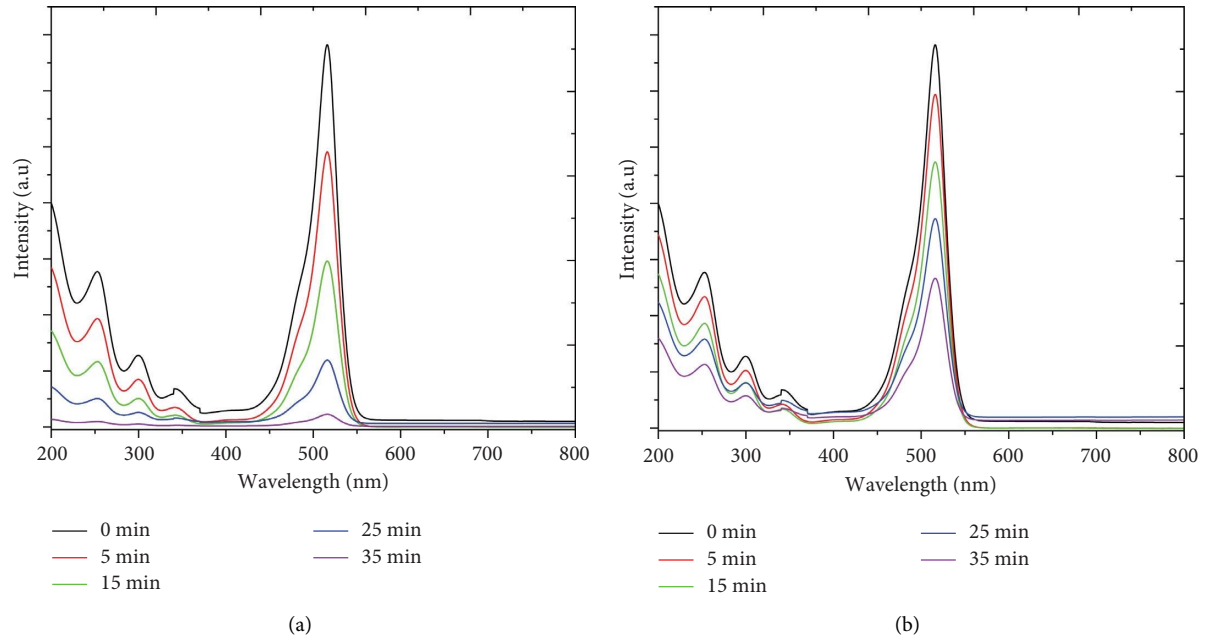

(a) (b)

Figure 6: Eosin yellowish degradation studies the effect of light exposure: (a) visible light and (b) UV light.

Furthermore, exceeding the ideal photocatalyst concentration could cause nanoparticle coagulation, resulting in less surface area and, thus, less photon retention, slowing the rate of photocatalyst degradation [38, 40–42].

2.4.4. Effect of Temperature. The solubility and mobility of dye molecules increase as the temperature rises, allowing them to interact more effectively with the active sites on the adsorbents' surfaces. The dissolved oxygen in the solution decreases when the temperature rises, which prevents the nanoparticles from oxidizing. A dye molecule's penetration is also enhanced by temperature, which affects activation energy and swelling within the adsorbent structure [43]. Eosin yellowish degradation was observed at 45°C (Figure 7(c)). Other researchers have found a similar effect of temperature on dye decolorization. Increasing the dye solution temperature from 30 to 50°C results in maximum degradation of the dye [43, 44].

2.4.5. Effect of pH. The pH of the solution is one of the essential regulating parameters in dye degradation. The pH effect can be described using the catalyst's point of zero

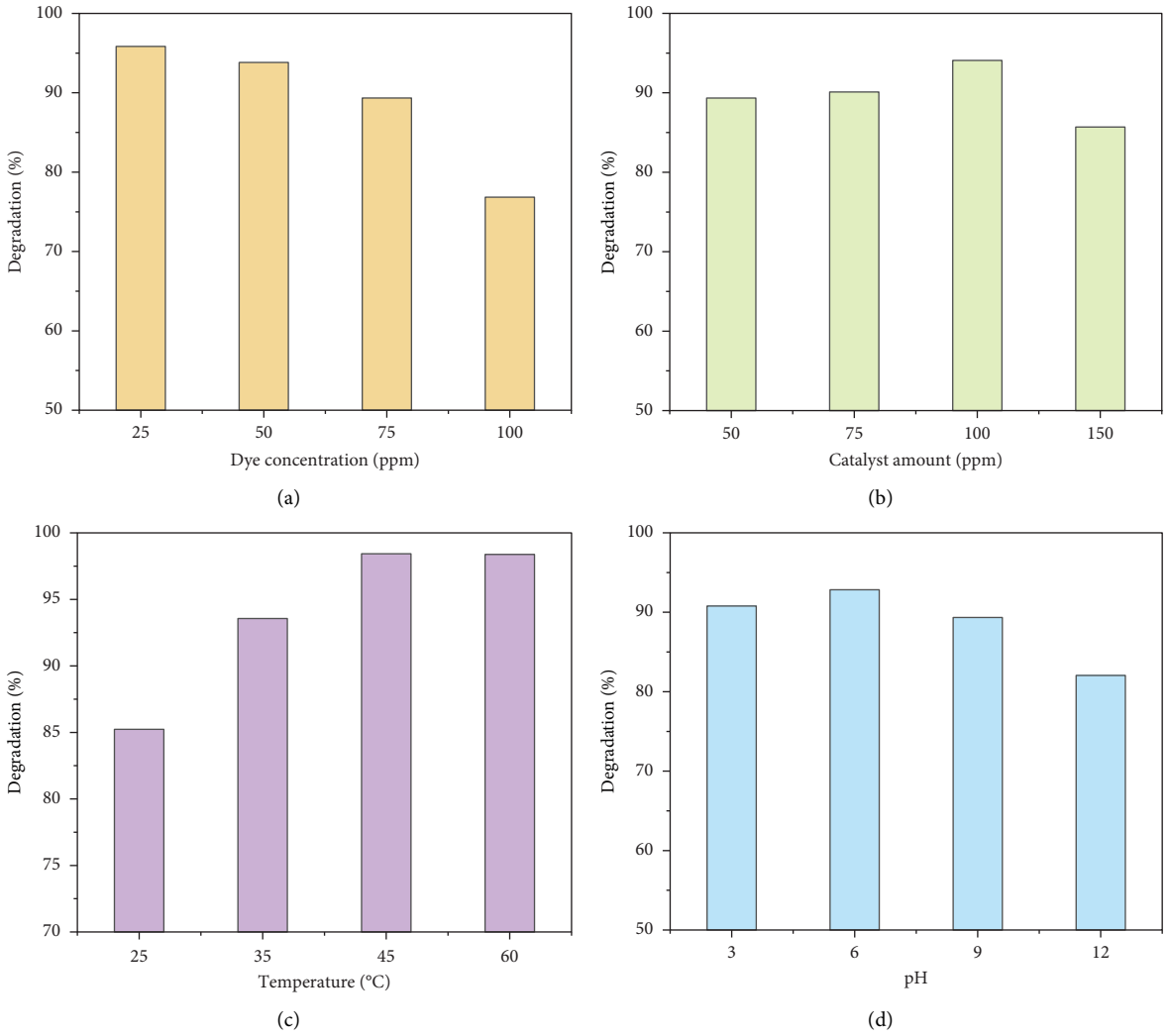

Figure 7: (a) Effect of dye concentration, (b) effect of catalyst dosage, (c) effect of temperature, and (d) effect of pH on eosin yellowish removable after 15 min exposure time.

charge. Synthetic Fe-oxides typically have a point of zero charge (PZC) between pH 7 and 9. When the pH falls below pHpzc, the catalyst surface becomes positively charged, favoring electrostatic interactions with anionic dyes. When the pH of cationic dye exceeds pHpzc, electrostatic interaction is observed [45]. This study assessed the effect of pH on the degradation of EY dye by Fe_2O_3 at 2, 6, 9, and 12 after 15 minutes (Figure 7(d)). The findings revealed that the efficiency of EY degradation is greater at pH 6 (10% greater than pH 12). It has been discovered. However, those hydroxyl radicals are formed due to the interaction of OH^- and h^+, essential oxidizing species at lower pH levels.

In contrast, hydroxyl radicals predominate at neutral or higher pH levels. High pH values generally prevent the retention of anionic dyes with a negative charge available on the photocatalyst's outer layer. As a result, it is strongly recommended that pH remain a pioneer in photocatalytic dye degradation [46–48].

2.4.6. Effect of Time. For 35 minutes, the effect of time exposure was studied for 100 ppm dye solution and 75 ppm nanoparticles. The absorbance peak was gradually reduced by increasing the time, as shown in Figure 8(a). After 35 minutes, the degradation of eosin reached nearly 100%. The following equation estimates the pseudofirst-order kinetics and kinetic rate constant:

$$-\ln\left(\frac{C0}{Ct}\right) = kt. \tag{4}$$

The curve is nearly linear curve fitting. The linear logarithm plot versus irradiation time indicates that the photodegradation reaction approximates first-order kinetics with a rate constant $(K) = 0.08\ \text{min}^{-1}$. Based on these "$k$" values, it can be confirmed that Fe_2O_3 has excellent photocatalytic activity (Figure 8(b)).

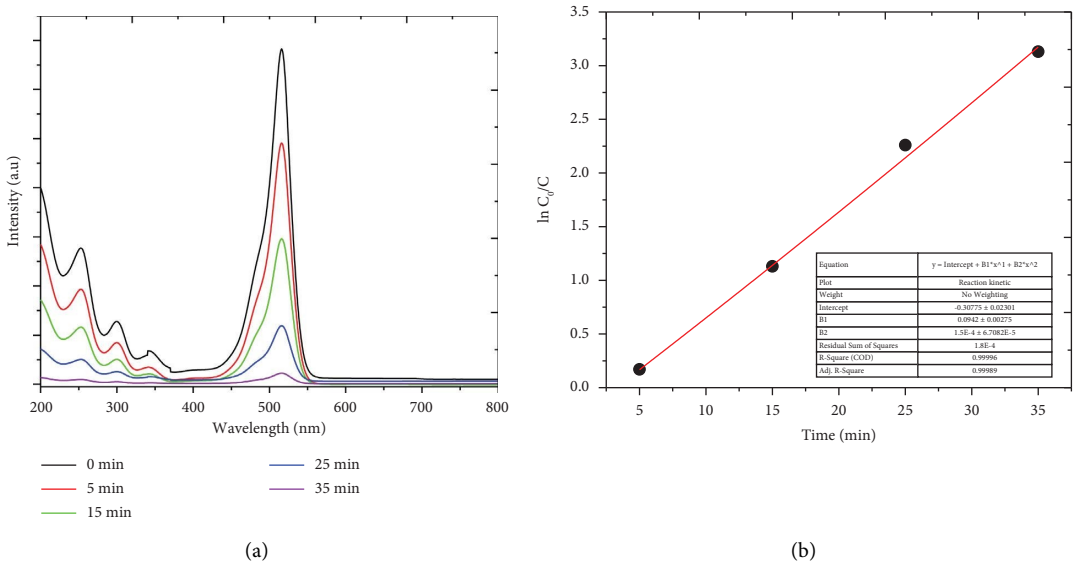

FIGURE 8: (a) Eosin yellowish degradation at different interval times and (b) the corresponding kinetic linear simulation curves ($\ln(C_0/C_t)$ vs. time).

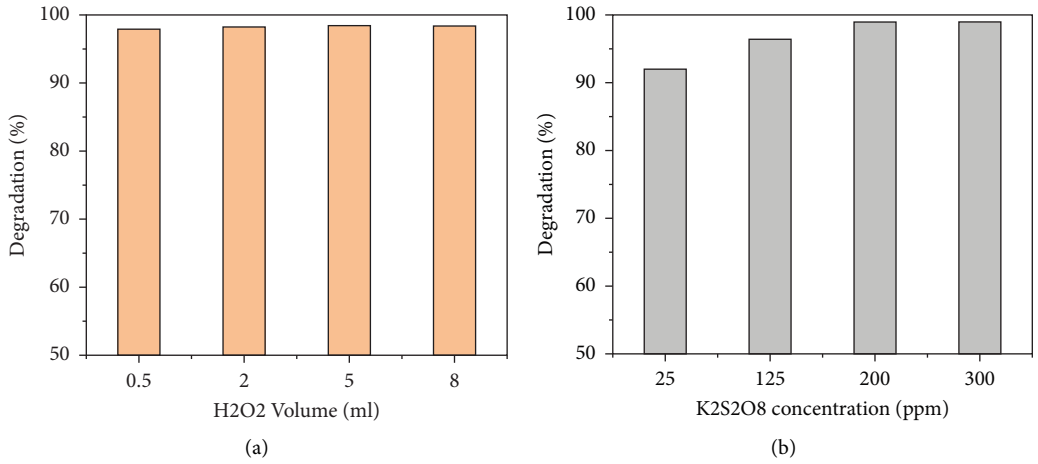

FIGURE 9: (a) Effect of hydrogen peroxide and (b) effect of potassium persulphate on eosin yellowish removable after 10 min exposure time.

2.4.7. Effect of Hydrogen Peroxide. According to photocatalytic degradation studies, H_2O_2 concentration is a critical variable that can significantly impact color removable. Adding H_2O_2 as an oxidant alongside visible light and Fe_2O_3 increased productivity significantly. When a light source with a frequency similar to hydrogen peroxide is absorbed, H_2O_2 produces •OH radicals (equations (5), (6). In the photooxidation cycle, a conjugation of Fe_2O_3 and H_2O_2 is required to achieve high efficiency in a short enlightenment period. The combination of light irradiation, H_2O_2, and Fe_2O_3 demonstrated the most excellent photodegradation rate (Figure 9(a)). •OH radicals produced on the catalyst's outer layer and those produced by the interaction of light and H_2O_2 oxidize dye molecules (equations (5), (6). As a result, experiments were conducted with differing volumes of H_2O_2 (30%) ranging from 0.5 to 8 ml at 75 ppm dye solution and 75 ppm catalyst. As shown in Figure 8(a), the initial rate of dye degradation increases significantly by ~90% without H_2O_2 and ~100% with H_2O_2. This aspect clearly explains the impact of H_2O_2 as an electron acceptor, as seen in equation (7), and may be due to a delay in the electron-hole recombination process following the generation of • OH by H_2O_2 on the consumption of an electron from the conduction band [49–55].

$$H_2O \longrightarrow \frac{1}{2}H_2 + \bullet OH \tag{5}$$

$$H_2O_2 \longrightarrow 2\bullet OH \tag{6}$$

$$Fe_2O_3\,(e^-) + H_2O_2 \longrightarrow OH\bullet + OH^- \tag{7}$$

2.4.8. Effect of Potassium Persulphate. The persulphate ion improves the efficiencies of EY photodegradation significantly. Figure 9(b) illustrates the influence of sodium

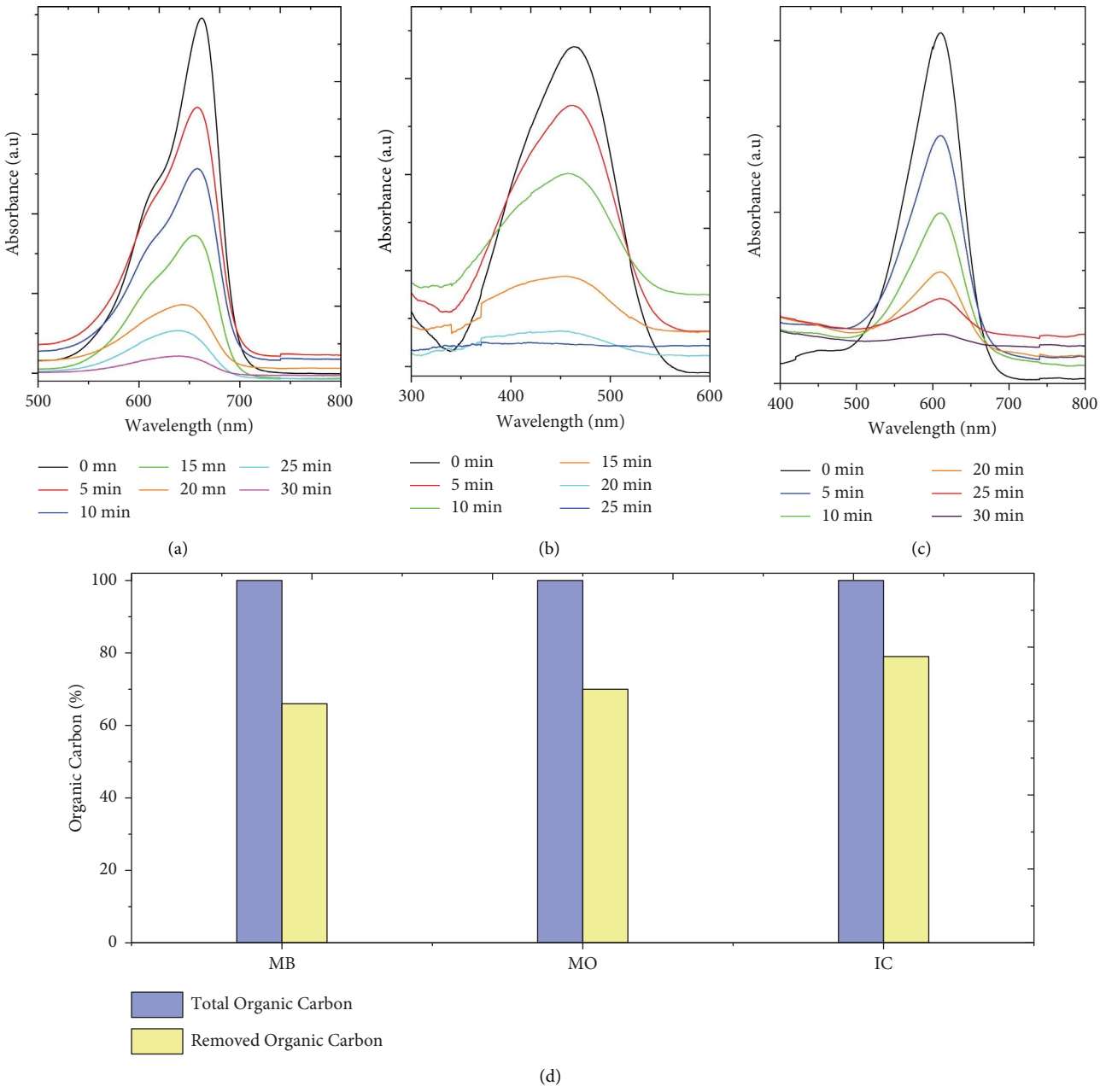

Figure 10: (a) MB, (b) MO, (c) IC degradation by PU-Fe_2O_3 membrane after, (d) organic carbon removable after 150 min (TOC data).

persulphate at concentrations ranging from 25 to 300 ppm. As the amount of $K_2S_2O_8$ increases, so does the rate of degradation of eosin. After 15 minutes of visible light irradiation, the 200 and 300 ppm $K_2S_2O_8$ were 100% removable. Because sodium persulphate acts as an electron trap, the reactive radical intermediate $SO_4^{\bullet -}$ is formed (equation (8)). The sulfate radical anion is a strong oxidizing agent that removes electrons from neutral molecules such as water and produces the hydroxyl radical (equation (9)).

$$Fe_2O_3\,(e^-) + S_2O_8^{2-} \longrightarrow SO_4^{\bullet -} + SO_4^{2-} \quad (8)$$

$$SO_4^{\bullet -} + H_2O \longrightarrow OH^{\bullet} + SO_4^{2-} + H^+ \quad (9)$$

Conversely, persulphate acts as an oxidant and an electron scavenger, preventing (e−/h+) recombination at the semiconductor surface. As a result, the faster photodegradation rate in the presence of persulphate ion is attributed to the formation of reactive sulfate radical anion, which generates a highly oxidative hydroxyl radical capable of removing the color molecules [11, 41, 56].

2.4.9. PU-Fe_2O_3Membrane-Based Photocatalysis for Dye Degradation. As a part of this study, we have successfully degraded methylene blue (MB), methyl orange (MO), and indigo carmine (IC) using square cut-upPU-Fe_2O_3, as we described above. As a result of the first cycle of treatment

with MB, the percentage of degradation was 89.23% (Figure 10(a)), while the percentage of degradation for the second cycle of treatment with MO was 91.23% (Figure 10(b)), and for the third cycle of treatment with IC was 83.51% (Figure 10(c)). Additionally, after 150 minutes of treatment under visible light, PU-Fe_2O_3 was able to remove 66% of carbon from MB, 70% from MO, and 79% from IC after 150 minutes of treatment under visible light (Figure 10(d)). Immobilizing iron nanoparticles on the polyurethane surface does not affect the catalytic performance of iron nanoparticles, but this material has the advantage of being reusable multiple times without difficulty.

3. Conclusion

According to the findings of this study, the initial dye concentration, catalyst dosage, pH, and exposure time all influenced the rate of degradation of eosin yellowish. For effective removal (95%) of 75 ppm eosin yellowish, 75 ppm Fe_2O_3 nanoparticles, and pH 6, a 15-minute exposure time is required. Furthermore, only 0.5 ml H_2O_2 (30% concentration) is required to increase eosin yellowish photocatalytic degradation. When $K_2S_2O_8$ was used, the same observation was made. Additionally, the reaction followed pseudofirst-order kinetics in terms of dye photo-removability. Also, the subsequent degradation of methylene blue, methyl orange, and indigo carmine with the PU-Fe_2O_3 membrane is almost as efficient as when the nanoparticles are used alone. As a result, the material can be readily degraded without any difficulties in removing and reusing it. Furthermore, an analysis of the total organic carbon (TOC) of the aforementioned dyes confirms the conclusions above.

Data Availability

All data have been included within the article.

Conflicts of Interest

The authors declare that they have no conflicts of interest.

Authors' Contributions

All authors contributed equally for data collection and manuscript writing.

Acknowledgments

This study was supported by the School of Engineering and Technology, National Forensic Sciences University.

References

[1] J. Wang, X. Shao, Q. Zhang, G. Tian, X. Ji, and W. Bao, "Preparation of mesoporous magnetic Fe_2O_3 nanoparticle and its application for organic dyes removal," *Journal of Molecular Liquids*, vol. 248, p. 13, 2017.

[2] G. Chaitanya Lakshmi, S. Ananda, R. Somashekar, and C. Ranganathaiah, "Synthesis of ZnO/MgO nanocomposites by electrochemical method for photocatalytic degradation kinetics of eosin Yellow dye," *International Journal of NanoScience and Nanotechnology*, vol. 3, pp. 47–63, 2012.

[3] Y. F. Sasaki, S. Kawaguchi, A. Kamaya et al., "The comet assay with 8 mouse organs: results with 39 currently used food additives," *Mutation Research, Genetic Toxicology and Environmental Mutagenesis*, vol. 519, no. 1-2, pp. 103–119, 2002.

[4] M. Pavlidis, T. Stupp, R. Naskar, C. Cengiz, and S. Thanos, "Retinal ganglion cells resistant to advanced glaucoma: a postmortem study of human retinas with the carbocyanine dye DiI," *Investigative Ophthalmology & Visual Science*, vol. 44, no. 12, pp. 5196–5205, 2003.

[5] S. Sharma, R. P. Goyal, G. Chakravarty, and A. Sharma, "Toxicity of tomato red, a popular food dye blend on male albino mice," *Experimental & Toxicologic Pathology*, vol. 60, no. 1, pp. 51–57, 2008.

[6] Dionex Corpration, "Note A Application Note 245 Fast HPLC Analysis of Dyes in Foods and Beverages," *Thermo Scientific*, Dionex.Corpration, Sunny value, CA, USA, 1986.

[7] A. Mittal, D. Jhare, and J. Mittal, "Adsorption of hazardous dye Eosin Yellow from aqueous solution onto waste material De-oiled Soya: isotherm, kinetics and bulk removal," *Journal of Molecular Liquids*, vol. 179, pp. 133–140, 2013.

[8] S. Bharathi, D. Nataraj, D. Mangalaraj, Y. Masuda, K. Senthil, and K. Yong, "Highly mesoporous α-Fe_2O_3 nanostructures: preparation, characterization and improved photocatalytic performance towards Rhodamine B (RhB)," *Journal of Physics D Applied Physics*, vol. 43, no. 1, Article ID 015501, 2010.

[9] S. Sakthivel, S. Geissen, D. W. Bahnemann, V. Murugesan, and A. Vogelpohl, "Enhancement of photocatalytic activity by semiconductor heterojunctions: Fe_2O_3, wo 3 and cds deposited on zno," *Journal of photochemistry and photobiology A: chemistry*, vol. 148, pp. 283–293, 2002.

[10] Y. L. Pang, S. Lim, H. C. Ong, and W. T. Chong, "Research progress on iron oxide-based magnetic materials: synthesis techniques and photocatalytic applications," *Ceramics International*, vol. 42, p. 34, 2016.

[11] H. Ansari, "Photochemical degradation of fluocinolone acetonidin drug in aqueous solutions using nanophotocatalyst zno doped by c," *North & South*, vol. 36, 2017.

[12] S. Balu, Y. L. Chen, R. C. Juang, T. C. K. Yang, and J. C. Juan, "Morphology-controlled synthesis of α–Fe_2O_3 nanocrystals impregnated on g-C_3N_4–SO_3H with ultrafast charge separation for photoreduction of Cr (VI) under visible light," *Environmental Pollution (Amsterdam, Netherlands)*, vol. 267, Article ID 115491, 2020.

[13] S. Balu, S. Velmurugan, S. Palanisamy et al., "Synthesis of α-Fe_2O_3 decorated g-C_3N_4/ZnO ternary Z-scheme photocatalyst for degradation of tartrazine dye in aqueous media," *Journal of the Taiwan Institute of Chemical Engineers*, vol. 99, pp. 258–267, 2019.

[14] S. K. Maji, N. Mukherjee, A. Mondal, and B. Adhikary, "Synthesis, characterization and photocatalytic activity of α-Fe_2O_3 nanoparticles polyhedron," *Polyhedron*, vol. 33, pp. 145–9, 2012.

[15] X. Liu, K. Chen, J. J. Shim, and J. Huang, "Facile synthesis of porous Fe_2O_3 nanorods and their photocatalytic properties," *Journal of Saudi Chemical Society*, vol. 19, no. 5, pp. 479–484, 2015.

[16] J. Deng, J. Liu, H. Dai, and W. Wang, "Preparation of α-Fe_2O_3 nanowires through electrospinning and their Ag_3PO_4 heterojunction composites with enhanced visible light photocatalytic activity," *Ferroelectrics*, vol. 528, no. 1, pp. 58–65, 2018.

[17] Z. Pu, M. Cao, J. Yang, K. Huang, and C. Hu, "Controlled synthesis and growth mechanism of hematite nano-rhombohedra, nanorods and nanocubes," *Nanotechnology*, vol. 17, no. 3, pp. 799–804, 2006.

[18] K. Woo, H. J. Lee, J. P. Ahn, and Y. S. Park, "Sol-gel mediated synthesis of Fe_2O_3 nanorods," *Advanced Materials*, vol. 15, pp. 1761–4, 2003.

[19] S. Mandal and A. H. E. Müller, "Facile route to the synthesis of porous α-Fe_2O_3 nanorods," *Materials Chemistry and Physics*, vol. 111, no. 2-3, pp. 438–443, 2008.

[20] P. R. Anusuyadevi, A. v. Riazanova, M. S. Hedenqvist, and A. J. Svagan, "Floating photocatalysts for effluent refinement based on stable pickering cellulose foams and graphitic carbon nitride (g-C_3N_4)," *ACS Omega*, vol. 5, no. 35, pp. 22411–22419, 2020.

[21] A. M. Nasir, J. Jaafar, F. Aziz et al., "A review on floating nanocomposite photocatalyst: fabrication and applications for wastewater treatment," *Journal of Water Process Engineering*, vol. 36, Article ID 101300, 2020.

[22] Z. Xing, J. Zhang, J. Cui et al., "Recent advances in floating TiO2-based photocatalysts for environmental application," *Applied Catalysis B: Environmental*, vol. 225, pp. 452–467, 2018.

[23] D. Zhang, F. Dai, P. Zhang, Z. An, Y. Zhao, and L. Chen, "The photodegradation of methylene blue in water with PVDF/GO/ZnO composite membrane," *Materials Science and Engineering: C*, vol. 96, pp. 684–692, 2019.

[24] K. Tan and S. K. Obendorf, "Development of an antimicrobial microporous polyurethane membrane," *Journal of Membrane Science*, vol. 289, no. 1-2, pp. 199–209, 2007.

[25] R. M. Kore and B. J. Lokhande, "A robust solvent deficient route synthesis of mesoporous Fe_2O_3 nanoparticles as supercapacitor electrode material with improved capacitive performance," *Journal of Alloys and Compounds*, vol. 725, pp. 129–138, 2017.

[26] W. Liu, J. Zhou, and J. Zhou, "Facile fabrication of multi-walled carbon nanotubes (MWCNTs)/α-Bi2O3 nanosheets composite with enhanced photocatalytic activity for doxycycline degradation under visible light irradiation," *Journal of Materials Science*, vol. 54, no. 4, pp. 3294–3308, 2019.

[27] C. Ding, L. Tian, B. Liu et al., "Facile in situ solvothermal method to synthesize MWCNT/$SnIn_4S_8$ composites with enhanced visible light photocatalytic activity," *Journal of Alloys and Compounds*, vol. 633, pp. 300–305, 2015.

[28] A. Rufus, N. Sreeju, and D. Philip, "Synthesis of biogenic hematite (α-Fe_2O_3) nanoparticles for antibacterial and nanofluid applications," *RSC Advances*, vol. 6, no. 96, pp. 94206–94217, 2016.

[29] A. Akbari, Z. Sabouri, H. A. Hosseini, A. Hashemzadeh, M. Khatami, and M. Darroudi, "Effect of nickel oxide nanoparticles as a photocatalyst in dyes degradation and evaluation of effective parameters in their removal from aqueous environments," *Inorganic Chemistry Communications*, vol. 115, Article ID 107867, 2020.

[30] N. Ashraf, M. Aadil, S. Zulfiqar et al., "Wafer-like cos architectures and their nanocomposites with polypyrrole for electrochemical energy storage applications," *Chemistry Select*, vol. 5, pp. 8129–36, 2020.

[31] L. Kumari, J. H. Lin, and Y. R. Ma, "One-dimensional Bi_2O_3 nanohooks: synthesis, characterization and optical properties," *Journal of Physics: Condensed Matter*, vol. 19, no. 40, Article ID 406204, 2007.

[32] W. F. Yao, H. Wang, X. H. Xu et al., "Sillenites materials as novel photocatalysts for methyl orange decomposition," *Chemical Physics Letters*, vol. 377, no. 5-6, pp. 501–506, 2003.

[33] S. Rackauskas, A. G. Nasibulin, H. Jiang et al., "A novel method for metal oxide nanowire synthesis," *Nanotechnology*, vol. 20, 2009.

[34] R. Atchudan, T. N. J. I. Edison, S. Perumal, D. Karthikeyan, and Y. R. Lee, "Facile synthesis of zinc oxide nanoparticles decorated graphene oxide composite via simple solvothermal route and their photocatalytic activity on methylene blue degradation," *Journal of Photochemistry and Photobiology B: Biology*, vol. 162, pp. 500–510, 2016.

[35] Y. Feng, N. Feng, Y. Wei, and G. Zhang, "An in situ gelatin-assisted hydrothermal synthesis of ZnO-reduced graphene oxide composites with enhanced photocatalytic performance under ultraviolet and visible light," *RSC Advances*, vol. 4, no. 16, pp. 7933–7943, 2014.

[36] M. Karimipour, M. Sadeghian, and M. Molaei, "Fabrication of white light LED photocatalyst ZnO–rGO heteronanosheet hybrid materials," *Journal of Materials Science: Materials in Electronics*, vol. 29, no. 16, pp. 13782–13793, 2018.

[37] M. Saquib and M. Muneer, "semiconductor mediated photocatalysed degradation of an anthraquinone dye remazol brilliant blue r under sunlight and artificial light source," *Dyes and Pigments*, vol. 53, 2002.

[38] A. Jegatha Christy and M. Umadevi, "Novel combustion method to prepare octahedral NiO nanoparticles and its photocatalytic activity," *Materials Research Bulletin*, vol. 48, no. 10, pp. 4248–4254, 2013.

[39] M. A. Gondal, T. A. Saleh, and Q. A. Drmosh, "Synthesis of nickel oxide nanoparticles using pulsed laser ablation in liquids and their optical characterization," *Applied Surface Science*, vol. 258, no. 18, pp. 6982–6986, 2012.

[40] M. A. Fox and M. T. Dulay, "Heterogeneous photocatalysis," *Chemical Reviews*, vol. 93, no. 1, pp. 341–357, 1993.

[41] D. Duraiswami and S. Revathi, "Photocatalytic degradation of tatrazine dye using TiO_2 catalyst: salt effect and kinetic studies," *Indian Journal of Chemical Technology*, vol. 14, 2007.

[42] F. Torki and H. Faghihian, "Photocatalytic activity of NiS NiO and coupled NiS-NiO for degradation of pharmaceutical pollutant cephalexin under visible light," *RSC Advances*, vol. 7, no. 86, pp. 54651–54661, 2017.

[43] A. Hamdy, M. K. Mostafa, and M. Nasr, "Zero-valent iron nanoparticles for methylene blue removal from aqueous solutions and textile wastewater treatment, with cost estimation," *Water Science and Technology*, vol. 78, no. 2, pp. 367–378, 2018.

[44] F. Luo, D. Yang, Z. Chen, M. Megharaj, and R. Naidu, "The mechanism for degrading Orange II based on adsorption and reduction by ion-based nanoparticles synthesized by grape leaf extract," *Journal of Hazardous Materials*, vol. 296, pp. 37–45, 2015.

[45] N. Sahu and K. M. Parida, "Photocatalytic Activity of Au/TiO_2 Nanocomposite for Azo-Dyes Degradation," *Kinetics And Catalysis*, vol. 53, pp. 197–205, 2012.

[46] N. Khandan Nasab, Z. Sabouri, S. Ghazal, and M. Darroudi, "Green-based synthesis of mixed-phase silver nanoparticles as an effective photocatalyst and investigation of their antibacterial properties," *Journal of Molecular Structure*, vol. 1203, Article ID 127411, 2020.

[47] K. Hayat, M. A. Gondal, M. M. Khaled, S. Ahmed, and A. M. Shemsi, "Nano ZnO synthesis by modified sol gel method and its application in heterogeneous photocatalytic

removal of phenol from water," *Applied Catalysis A: General*, vol. 393, no. 1-2, pp. 122–129, 2011.

[48] N. Daneshvar, D. Salari, and A. R. Khataee, "Photocatalytic degradation of azo dye acid red 14 in water on ZnO as an alternative catalyst to TiO_2," *Journal of Photochemistry and Photobiology A: Chemistry*, vol. 162, no. 2-3, pp. 317–322, 2004.

[49] A. L. Linsebigler, G. Lu, and J. T. Yates, "Photocatalysis on tion surfaces: principles, Mechanisms, and Selected Results," *Chemical reviews*, vol. 95, 1995.

[50] C. Kumar Singh, M. R. Hoffmann, S. T. Martin, W. Choi, and D. W. Bahnemannt, "Environmental applications of semiconductor photocatalysis," *Chemical reviews*, vol. 95, 1995.

[51] A. Fujishima, T. N. Rao, and D. A. Tryk, "Titanium dioxide photocatalysis," *Journal of photochemistry and photobiology C: Photochemistry reviews*, vol. 1, 2000.

[52] S. R. Cater, M. I. Stefan, J. R. Bolton, and A. Safarzadeh-Amiri, "UV/H2O2 treatment of methyl tert-butyl ether in contaminated waters," *Environmental Science & Technology*, vol. 34, no. 4, pp. 659–662, 2000.

[53] S. Parra, V. Sarria, S. Malato, P. Péringer, and C. Pulgarin, "Photochemical versus coupled photochemical-biological flow system for the treatment of two biorecalcitrant herbicides: metobromuron and isoproturon," *Applied Catalysis B: Environmental*, vol. 27, 2000.

[54] M. I. Stefan and J. R. Bolton, "Reinvestigation of the acetone degradation mechanism in dilute aqueous solution by the UV/H_2O_2 process," *Environmental Science & Technology*, vol. 33, no. 6, pp. 870–873, 1999.

[55] V. K. Gupta, R. Jain, A. Mittal, M. Mathur, and S. Sikarwar, "Photochemical degradation of the hazardous dye Safranin-T using TiO_2 catalyst," *Journal of Colloid and Interface Science*, vol. 309, no. 2, pp. 464–469, 2007.

[56] L. M. Ahmed, S. I. Saaed, and A. A. Marhoon, "Effect of oxidation agents on photo-decolorization of vitamin B_{12} in the presence of ZnO/UV-A system," *Indonesian Journal of Chemistry*, vol. 18, no. 2, pp. 272–278, 2018.